

Metal-Insulator transition and Charge Transport Mechanisms in SnSe₂ Field-Effect Transistor

Aarti Lakhara,¹ Lars Thole,² Rolf J. Haug,² and P. A. Bhobe¹

¹*Department of Physics, Indian Institute of Technology Indore, Khandwa Road, Indore, Simrol, 453552, India*

²*Institut für Festkörperphysik, Leibniz Universität Hannover, 30167 Hannover, Germany*

(*Electronic mail: pbhobe@iiti.ac.in)

(*Electronic mail: haug@nano.uni-hannover.de)

(Dated: 22 July 2025)

We report an observation of metal-insulator transition in a thin film of SnSe₂. The room-temperature carrier concentration of SnSe₂ film was increased by electrostatic doping to $1.14 \times 10^{13} \text{ cm}^{-2}$. A crossover from insulating phase to metallic state was clearly observed. The low-temperature charge transport mechanism is governed by two-dimensional (2D) variable-range hopping. This mechanism is influenced by band bending and gap states introduced by selenium vacancies. At low temperatures, the mobility is primarily limited by charged impurities, while at higher temperatures, it follows a power-law dependence, $\mu = T^{-\gamma}$, indicating a dominance of electron-phonon scattering. The application of a gate field shifts the Fermi level toward the conduction band, and at sufficiently high temperatures, this drives the system into a metallic state. Our findings offer insights into the charge transport mechanisms in SnSe₂ FET, this understanding will allow for the optimization of other 2D materials for advanced electronic device applications.

SnSe₂, a semiconductor belonging to the group of *s-p* metal dichalcogenides, has garnered significant attention in recent years due to its exotic quantum phases such as charge density waves¹, and superconductivity^{2,3}. Alongside its varied quantum phases, SnSe₂ possesses a band gap of approximately 1 eV, which is comparable to silicon (1.1 eV), thereby highlighting its potential for optoelectronic applications⁴. Since 2013, SnSe₂ has been investigated extensively as a channel material for field-effect transistors (FETs). Some of the recent results include a 25 nm thick device that exhibits a persistent conductive state even under substantial negative back-gate voltages, indicating a high electron concentration⁵. Furthermore, placing a top capping layer of polymer electrolyte on a 10 nm thick FET⁶ was seen to help achieve a current on/off ratio of 10^4 . In another study, a 84 nm thick device had been found to demonstrate a high room temperature drive current of $160 \mu\text{A}/\mu\text{m}^7$, placing it in competition with other high-performance 2D - based FETs⁸.

While SnSe₂-based FETs have been extensively explored for practical applications, the fundamental physics governing charge transport mechanisms in this material remain unclear. The present study aims at investigating the temperature and electric field-dependent transport characteristics of a 11.8 nm (~ 19 layer) thick SnSe₂ FET fabricated on SiO₂/Si substrate through simple exfoliation method. Multi-layer configurations are advantageous as they are less influenced by the substrate compared to monolayers, facilitating extraction of intrinsic material properties in lower dimensions. Mobility serves as a key metric for FET devices, and SnSe₂ FETs have shown high mobility, for example, $85 \text{ cm}^2/\text{Vs}$ at room temperature for an 8.6 nm thick device⁹. The present investigation thus covers field effect mobilities (μ_{FE}) and transfer curves of SnSe₂ across a temperature range from 10 K to 300 K. Our back-gated device demonstrates a high mobility of $128 \text{ cm}^2/\text{Vs}$ at 300 K, surpassing previously reported values in the literature. Furthermore, the field-effect mobility

increases as the temperature decreases, reaching a maximum of approximately $387 \text{ cm}^2/\text{Vs}$ at 60 K and starts to decrease with further decrease in temperature. Our analysis effectively demonstrates that the decrease is due to static charge vacancies present in the system, which are responsible for variable range hopping (VRH) transport in the low temperature range. Interestingly, the VRH insulating state transforms into a metallic state above 120 K, due to increase in carrier concentrations ($> 6.66 \times 10^{12} \text{ cm}^{-2}$) induced by back-gate voltage.

The SnSe₂ single crystals were grown by chemical vapor transport (CVT) method (see supplementary material Sec. S1). The elemental mapping and EDX spectra were recorded on bulk crystal to confirm the homogeneity (see supplementary material Sec. S2). An atomic ratio of Sn:Se = 1:1.95 is obtained in synthesized crystals. The XRD profile of SnSe₂, shown in Fig. 1(a) is an expression of its single crystalline nature that displays highly oriented (00*l*) planes and very low intensities of other planes. All the observed peaks are indexed to CdI₂ type hexagonal unit cell with *P-3m1* space group, confirming the phase purity of the composition. Using the Le Bail method integrated within the FullProf suite^{10,11}, we carried out the refinement of the XRD profile and extracted the lattice parameters values as, $a = b = 3.857 \text{ \AA}$ and $c = 6.147 \text{ \AA}$, that match well with previous reports¹². Fig. 1(b) shows the Raman spectra of SnSe₂, where in-plane vibrational mode (E_g), and out-of-plane vibrational mode (A_{1g}) are located at 110 cm^{-1} and 185 cm^{-1} respectively. Similar to other dichalcogenides, the Sn atom in SnSe₂ is sandwiched between two Se atoms, and it crystallizes in two polytypes: 2H (space group $P\bar{3}m1$, D_{3d}^4 , 164) and 1T (space group $P6_3/mmc$, D_{6h}^4 , 194). The peak position of the E_g mode at 110 cm^{-1} confirms the 2H polytype^{13,14} in the SnSe₂ single crystals synthesized here. The SnSe₂ FET device was fabricated using standard mechanical exfoliation method (details of device fabrication can be found in supplementary material Sec. S3). The AFM image of fabricated SnSe₂ FET is presented in Fig. 2(a). The ohmic-

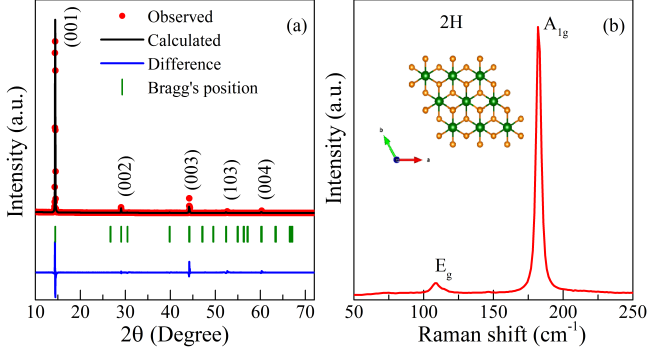


FIG. 1. (a) Le Bail refined XRD pattern of SnSe₂. (b) Room temperature Raman spectra of SnSe₂ single crystal and inset shows 2H structure of SnSe₂.

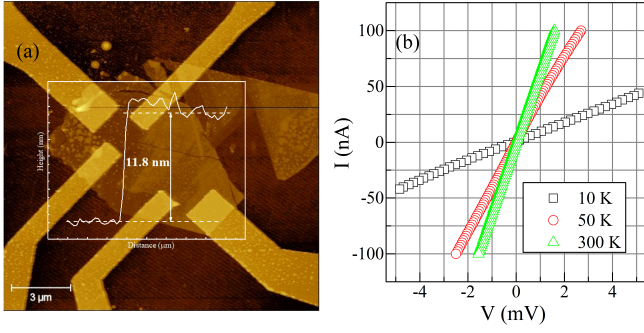


FIG. 2. (a) Atomic force microscopy image of SnSe₂ thin flake with height profile of the flake, showing a thickness of 11.85 nm. (b) Temperature-dependent I-V curve, demonstrating good electrical contact.

contact is formed as confirmed through I-V curve measurement (see Fig. 2(b)).

We begin by investigating the characteristics of the electronic states of the SnSe₂ channel. For this, we conduct temperature-dependent four-point resistance measurements with the back-gate voltage set to 0 V and 70 V, as shown in Fig. 3. At 0 V in Fig. 3 (a), SnSe₂ exhibits semiconductor behavior, consistent with its intrinsic nature^{15,16}. With increasing temperature the resistance drops sharply until ~ 30 K, followed by a gradual decrease until ~ 150 K, and thereafter remains constant irrespective of the temperature change.

As seen in Fig. 3(b), the low temperature data is best described by Variable Range Hopping (VRH) transport mechanism¹⁷, showing a straight-line dependence between $\ln(\sigma)$ and $T^{-1/3}$, where σ is the conductivity. In VRH transport mechanism electrons hop between occupied localized states and free localized states. These localized states are spatially separated but have equivalent energies, and they exist within the band gap of the material. In SnSe₂, these "gapped" states can be intrinsic, arising from charge defects in the crystal, or extrinsic, due to the metal-semiconductor interface formed at the electrical contacts. Given the high electron affinity of SnSe₂¹⁸, electrons flow from the metal contact (Cr/Au), leading to band bending at the interface and poten-

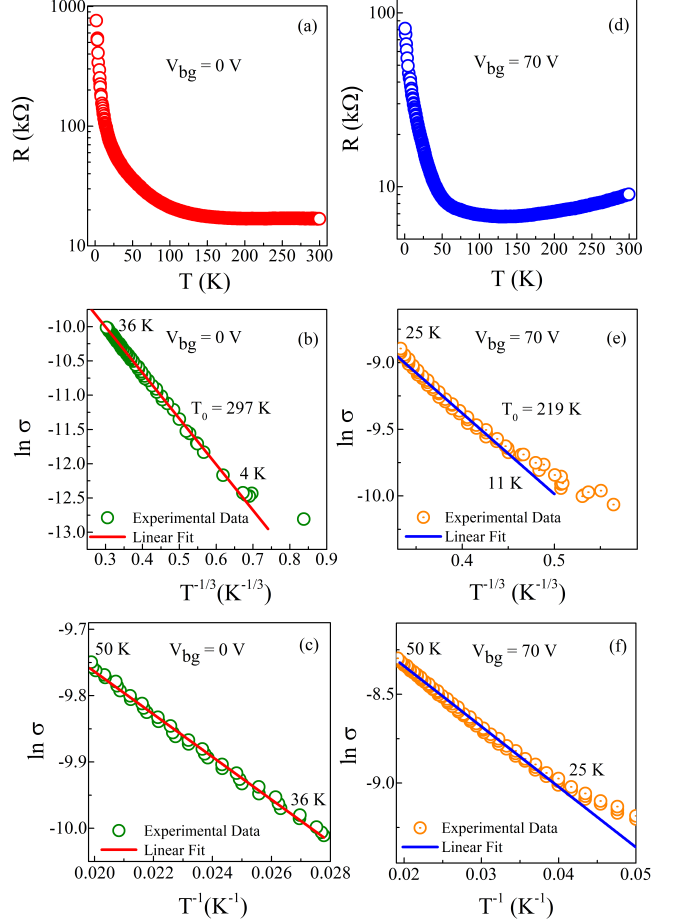


FIG. 3. (a) Four-point resistance as a function of temperature at zero back-gate voltage. (b) $\ln \sigma$ as function of $T^{-1/3}$. Symbols represent experimental data, and the red line shows a linear fit from 36 K to 5 K, indicating a 2D VRH transport mechanism. (c) $\ln \sigma$ as a function of $1/T$ from 36 K to 50 K, suggesting a transition to nearest-neighbour hopping transport. (d) Four-point resistance as a function of temperature at a 70 V back-gate voltage. (e) represent the 2D VRH for 70 V back-gate voltage from 25 K to 11 K. (f) From 25 K to 50 K nearest-neighbour hopping describe the transport mechanism very well for 70 V back-gate voltage.

tially contributing to gapped states. Additionally, recent electronic structure calculations of SnSe₂ show that Se vacancies induce several peaks in the gapped region of the density of states, closely linked to the formation of gapped states that activate new transitions in the optical spectrum¹⁹. The given Sn:Se ratio of 1:1.95 in the synthesized crystal corresponds to approximately 2.5% Se vacancies. These vacancies are significant enough to contribute to the formation of impurity levels close to the conduction band, which in turn lead to the observed variable-range hopping (VRH) conduction at low temperatures. VRH occurs through these states, and is described by the relation $\sigma \propto \exp[-(T_0/T)^{1/(d+1)}]$, where T_0 is the characteristic temperature and d is the dimensionality of the system. From the fitting, we obtain the characteristic temperature $T_0 \sim 297$ K. Given the 2D nature of SnSe₂ crystals, our data fits well for $d = 2$, indicating that the electrical transport is

confined only in the $x - y$ plane. In the intermediate temperature range, where resistance changes gradually, the transport follows the nearest neighbour hopping (NNH) mechanism described by the relation, $\sigma \propto \exp(-E_a/k_B T)$, where E_a is the activation energy and k_B is the Boltzmann constant. Accordingly, $\ln(\sigma)$ varies linearly with $1/T$, as shown in Fig. 3(c).

With the back-gate voltage set at 70 V, the shape of the resistance versus temperature curve remains largely unchanged in the low temperature range. However, the magnitude of resistance decreases significantly compared to 0 V data. Another noticeable change is the increase in resistance with rising temperature, beyond ~ 120 K, a behavior characteristic of metallic conduction, as can be seen in Fig. 3(d). Accordingly, for temperatures below 25 K, conductivity fits the VRH mechanism, followed by the NNH mechanism until 50 K. Beyond the NNH regime, the effect of rising thermal energy is seen to affect the conduction process. The data here fits an activation transport behavior (as will be discussed further), until metallic state is reached beyond ~ 120 K.

To gain more insight into the metal-insulator transition (MIT), we examine the temperature-dependent conductance behavior with systematic increase in the back-gate voltages. The conductance (G) measured by sweeping the back-gate voltage in the range ∓ 70 V and at various fixed temperatures, ranging from 1.7 K to 300 K, is shown in Fig. 4(a). As depicted in these plots, conduction predominantly occurs in the positive back-gate region, indicating the intrinsic n -type nature of SnSe₂²⁰. The corresponding plot of conductance versus temperature (derived from Fig. 4(a)) at various fixed back-gate voltages, is shown in Fig. 4(b).

We calculated the 2D carrier density (n_{2D}) of SnSe₂ as, $n_{2D} = C_{ox} \frac{\Delta V_{bg}}{e}$, where C_{ox} is given by $\epsilon_0 \epsilon_r / d$, where $\epsilon_0 = 8.85 \times 10^{-12} \text{ Fm}^{-1}$, $\epsilon_r = 3.9$ for SiO₂, $d = 340$ nm is the thickness of SiO₂ layer, and $\Delta V_{bg} = V_{bg} - V_{th}$ where V_{th} is the threshold value of back-gate voltage beyond which a distinct rise in conductance with increasing back-gate voltage is observed. At room temperature, n_{2D} increases from $7.04 \times 10^{12} \text{ cm}^{-2}$ at 0 V to $1.14 \times 10^{13} \text{ cm}^{-2}$ at 70 V. The minimum back-gate voltage of 10 V, where the metallic behavior seems to occur at a much higher temperature (≥ 300 K) corresponds to carrier concentration $6.66 \times 10^{12} \text{ cm}^{-2}$. This value of n_{2D} is of the same order as that observed in MoS₂, where the MIT is reported to occur at $\sim 1 \times 10^{13} \text{ cm}^{-2}$ in the presence of a high dielectric environment²¹. As the back-gate voltage is increased, the transition temperature that marks a change in conductance from an insulating type to metallic type, decreases systematically. A dashed line in Fig. 4(b) is a guide to the eye, demonstrating the variation of MIT from 300 K for $V_{bg} = 10$ to 120 K at $V_{bg} = 70$ V.

To get further insight into the charge transport mechanism, the field-effect mobility is extracted from the conductance curve in the 50-70 V range of back-gate voltage, using the expression ,

$$\mu = \frac{L}{W} \left(\frac{1}{C_{ox}} \right) \frac{dG}{dV_{bg}}$$

Here L, W are length and width of channel, respectively. As shown in Fig. 4(c), the temperature dependence of mobility

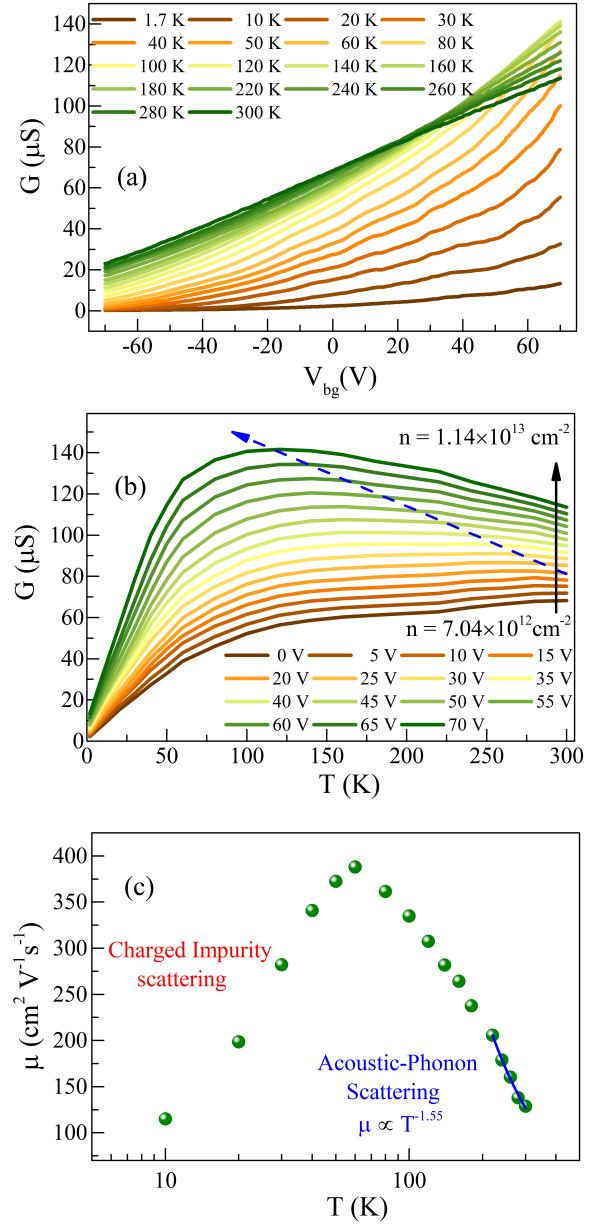


FIG. 4. (a) Conductance (G) as a function of back-gate voltage (transfer characteristics) at various temperatures. (b) Conductance as a function of temperature for back-gate voltages ranging from 0 V to 70 V. The dashed blue arrow is a guide to eye, showing the metal-insulator transition. (c) Variation of mobility with temperature.

exhibits a distinct peak, indicating a characteristic transport mechanism within the system. The maximum mobility value of $387 \text{ cm}^2/\text{Vs}$ is reached at 60 K, and decreases thereafter as temperature increases, reaching a value of $128 \text{ cm}^2/\text{Vs}$ at room temperature. The temperature dependence of mobility indicates an electron-phonon scattering mechanism at play. Indeed, a power-law fit to the mobility data at elevated temperatures, expressed as $\mu = T^{-\gamma}$, yields an exponent $\gamma = 1.55$. This value closely aligns with the temperature dependence for acoustic-phonon scattering, $\mu \propto T^{-1.5}$, suggesting it to be the

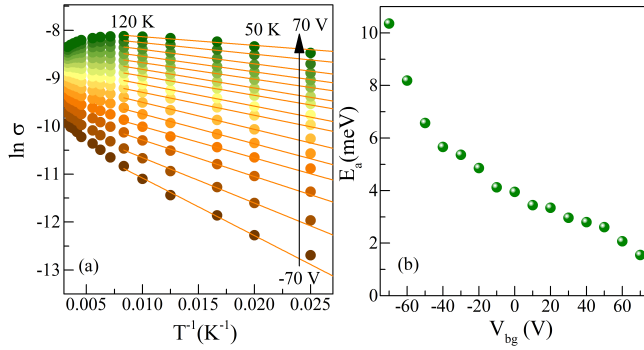


FIG. 5. (a) A plot demonstrating the thermally activated transport behaviour in conductance measured at various back-gate voltages in the intermediate temperature regime. (b) Variation in the activation energy with back-gate voltage.

dominant phenomenon at high temperatures. With a decrease in temperature, the mobility values deviate from the power-law fit, indicating that additional scattering mechanisms may be playing a role in the transport properties of SnSe_2 .

Previously, the analysis of the resistance versus temperature curve obtained for the back-gate voltage set at 70 V, indicated that thermally activated transport occurs in the intermediate temperature range. Accordingly, the data extracted from Fig. 4(a), and presented as $\ln(\sigma)$ versus temperature in Fig. 5(a), conveys a linear relationship in the temperature range $50 \text{ K} \leq T \leq 120 \text{ K}$. The extracted values of activation energy (E_a) seem to decrease as the back-gate voltage increases (see Fig. 5(b)), indicating a clear influence of the back-gate voltage on the electronic states. As a result of accumulated electrons caused by the field effect, donor energy levels below the conduction band become filled, leading to a shift in the Fermi level. From the plot, it is clear that this shift occurs from 10.35 meV to 1.55 meV. Consequently, SnSe_2 become more conductive at 70 V back-gate voltage.

Hence, transition of SnSe_2 from an insulating to a metallic state is observed with the application of back-gate voltage. With $\sim 2.5\%$ Se vacancies in the system, their random distribution creates a rough potential landscape for the electrons, contributing to the formation of gapped states between the valance and conduction band edges. At low carrier density, electrons are unable to screen this potential fluctuation, and the transport occurs through the hopping mechanism in the insulating regime. As the carrier density increases through the field effect, electrons can screen the disorder potential more effectively. We observe that the screening ability is sensitive to temperature. The application of back-gate voltage introduces more electrons into the sample, thereby increasing the carrier concentration. As the back-gate voltage is systematically increased, the Fermi level shifts closer to the conduction band, reducing the thermal energy required to excite charge carriers. This effect is reflected in the observed decrease in activation energy with increasing back-gate voltage.

In conclusion, we conduct a comprehensive investigation of charge transport phenomena in a 19 layers (11.85 nm) thin SnSe_2 FET device. We explore the transport characteristics

over a broad range of carrier densities, which are tuned by applying back-gate voltages. Notably, we report a metal-insulator transition in SnSe_2 at high carrier densities, occurring between 120 K and 300 K. Our analysis indicate that charge impurity scattering dominates the mobility at low temperatures, while phonon scattering becomes the predominant mechanism at higher temperatures in the presence of field effect. Based on our findings, we demonstrate that the phase transition in SnSe_2 can be controlled by modulating the carrier density and temperature alone, without the need for complex device architectures. This suggests potential applications where SnSe_2 can function as both the semiconducting channel and metallic interconnects, offering a solution to challenges such as band mismatches and Schottky barriers commonly encountered in 2D material-based FETs.

ACKNOWLEDGMENTS

This work was supported by German Academic Exchange Service (DAAD) funded project LUH-IIT Indore Partnership (2019-2023) under the ‘‘A New Passage to India program’’. Aarti lakhara acknowledges DST-INSPIRE (File: DST/INSPIRE/03/2019/001146/IF190704), New Delhi, for providing the research fellowship. Work at Leibniz University Hannover was funded by the Deutsche Forschungsgemeinschaft (DFG, German Research Foundation) under Germany’s Excellence Strategy - EXC 2123 Quantum Frontiers - 390837967 and within the Priority Program SPP 2244 ‘2DMP’. We also acknowledges Department of Science & Technology, India, for its support through FIST project (SR/FST/PSI-225/2016) for the establishment of Raman spectroscopy measurement system at the Department of Physics, IIT Indore.

I. AUTHOR DECLARATIONS

Aarti Lakhara and Lars Thole contributed equally to this work.

A. Conflict of Interest

The authors have no conflicts to disclose.

B. Author Contributions

Aarti Lakhara: Conceptualization (equal); Data curation (equal); Investigation (equal); Writing – original draft; Writing – review & editing (equal).

Lars Thole: Conceptualization (equal); Investigation (equal); Formal analysis (equal); Writing – review & editing (equal).

Rolf J. Haug: Conceptualization (equal); Formal analysis (equal); Writing – review & editing (equal); Resources (equal); Supervision; Funding acquisition (lead).

P. A. Bhohe: Conceptualization (equal); Formal analysis (equal); Writing – review & editing (equal); Resources (equal); Supervision; Funding acquisition (lead).

DATA AVAILABILITY STATEMENT

The data that support the findings of this study are available from the corresponding authors upon reasonable request.

- ¹S.-Z. Wang, Y.-M. Zhang, J.-Q. Fan, M.-Q. Ren, C.-L. Song, X.-C. Ma, and Q.-K. Xue, *Phys. Rev. B* **102**, 241408 (2020).
- ²Y.-M. Zhang, J.-Q. Fan, W.-L. Wang, D. Zhang, L. Wang, W. Li, K. He, C.-L. Song, X.-C. Ma, and Q.-K. Xue, *Phys. Rev. B* **98**, 220508 (2018).
- ³L. K. Ma, M. Z. Shi, B. L. Kang, K. L. Peng, F. B. Meng, C. S. Zhu, J. H. Cui, Z. L. Sun, D. H. Ma, H. H. Wang, B. Lei, T. Wu, and X. H. Chen, *Phys. Rev. Mater.* **4**, 124803 (2020).
- ⁴G. Domingo, R. S. Itoga, and C. R. Kannewurf, *Phys. Rev.* **143**, 536 (1966).
- ⁵T. Pan, D. De, J. Manongdo, A. Guloy, V. Hadjiev, Y. Lin, and H. Peng, *Appl. Phys. Lett.* **103**, 093108 (2013).
- ⁶T. Pei, L. Bao, G. Wang, R. Ma, H. Yang, J. Li, C. Gu, S. Pantelides, S. Du, and H.-j. Gao, *Appl. Phys. Lett.* **108**, 053506 (2016).
- ⁷Y. Su, M. A. Ebrish, E. J. Olson, and S. J. Koester, *Appl. Phys. Lett.* **103**, 263104 (2013).
- ⁸H. Abuzaid, N. X. Williams, and A. D. Franklin, *Appl. Phys. Lett.* **118**, 030501 (2021).
- ⁹C. Guo, Z. Tian, Y. Xiao, Q. Mi, and J. Xue, *Appl. Phys. Lett.* **109**, 203104 (2016).
- ¹⁰A. Le Bail, H. Duroy, and J. L. Fourquet, *Mater. Res. Bull.* **23**, 447 (1988).
- ¹¹J. Rodríguez-Carvajal, *Physica B: Condens. Matter.* **192**, 55 (1993).
- ¹²A.-T. Pham, T. H. Vu, C. Cheng, T. L. Trinh, J.-E. Lee, H. Ryu, C. Hwang, S.-K. Mo, J. Kim, L.-d. Zhao, *et al.*, *ACS Appl. Energy Mater.* **3**, 10787 (2020).
- ¹³R. Biswas, M. Dandu, A. Prosad, S. Das, S. Menon, J. Deka, K. Majumdar, and V. Raghunathan, *Sci. Rep.* **11**, 15017 (2021).
- ¹⁴M. Mandal, N. Maity, P. K. Barman, R. Biswas, S. Mondal, V. Raghunathan, A. K. Singh, P. K. Nayak, and K. Sethupathi, *Phys. Rev. B* **110**, 195404 (2024).
- ¹⁵J. Ying, H. Paudyal, C. Heil, X.-J. Chen, V. V. Struzhkin, and E. R. Margine, *Phys. Rev. Lett.* **121**, 027003 (2018).
- ¹⁶I. Pallecchi, F. Caglieris, M. Ceccardi, N. Manca, D. Marré, L. Repetto, M. Schott, D. I. Bile, S. Chaitoglou, A. Dimoulas, and M. J. Verstraete, *Phys. Rev. Mater.* **7**, 054004 (2023).
- ¹⁷N. F. Mott, *Philos. Mag.* **19**, 835 (1969).
- ¹⁸Q. Zhang, M. O. Li, E. B. Lochocki, S. Vishwanath, X. Liu, R. Yan, H.-H. Lien, M. Dobrowolska, J. Furdyna, K. M. Shen, *et al.*, *Appl. Phys. Lett.* **112** (2018).
- ¹⁹H. Zhong, J. Yu, X. Kuang, K. Huang, and S. Yuan, *Phys. Rev.* **101**, 125430 (2020).
- ²⁰B. Evans and R. Hazelwood, *J. Phys. D Appl. Phys.* **2**, 1507 (1969).
- ²¹B. Radisavljevic and A. Kis, *Nat. Mater.* **12**, 815 (2013).